

## Influence of soil surface roughness on soil bidirectional reflectance

J. CIERNIEWSKI

Adam Mickiewicz University, Institute of Physical Geography, Fredry 10,  
61-701 Poznan, Poland

M. VERBRUGGHE

I.N.R.A., Bioclimatologie, B.P. 91, 84143 Montfavet, France

(Received 5 March 1996; in final form 12 August 1996)

**Abstract.** The non-Lambertian behaviour of soil surfaces depends on its roughness at micro-scale and larger scales, as well as on the incident angle of the direct solar beam on the surface. A geometrical model, taking into account the diffuse as well as the specular component of energy leaving soil surfaces in the visible and near-infrared, is used in the paper to describe the influence of soil surface roughness, caused by soil aggregates or soil clods, on the soil bidirectional reflectance distribution. A rough soil surface in the model is simulated by equal-sized opaque spheroids lying on a horizontal surface. The model was tested in outdoor conditions on artificially formed soil surfaces made of two spectrally different soil materials: a mineral loam, and a loam with high organic matter content. The spectral data were measured by a field radiometer in the three SPOT (HRV) bands. The model predicts that at specific illumination conditions, soils surfaces with the highest roughness, expressed by the minimum distances between soil aggregates, can show lower variation of reflectance in the view zenith angle function than soil surfaces of a lower roughness.

### 1. Introduction

Soils, like many natural objects, show variation in their radiance due to the direction of irradiating solar energy and the direction along which the reflected energy is detected. Rough soil surfaces usually display a clear backscattering character with a backscatter reflectance peak towards the Sun position, and decreasing reflectance in the direction away from the peak, with minimum reflectance in the extreme forwardscatter direction near the horizon (Kimes and Sellers 1985, Milton and Webb 1987; Ott *et al.*, 1984). The peak of backscattering radiation becomes less pronounced as the solar zenith angle decreases. Deering *et al.* (1990) showed evidence that soil reflectance could clearly have both a backscattering and a forward scattering character. The forward scatter regime demonstrated a surface composed of nearly pure gypsum crystals creating uniform wind ripples.

The non-Lambertian behaviour of a soil surface depends on its roughness at micro-scale and larger scales, as well as on the incident angle of the direct solar beam on the surface. If the surface in micro-scale is smooth in relation to the wavelength, the sunbeams are reflected specularly. Electromagnetic field reflected in this way is polarized. The higher the incident angle from the normal to the surface, the higher polarization of light according to the Fresnel equation (Mulders 1987). The pattern of the specular re-radiation is directional, where the angle of incidence equals the angle of reflection. If the soil surface in micro-scale is rough, the direct

solar beam falling on the surface is dispersed into vectors creating the ideal shape of a sphere, independent of the angle of incidence. The criterion of roughness to divide between smooth and rough particle surfaces in micro-scale depends on wavelength and the incidence angle of the direct solar beam. Taking into account the extreme wavelengths of the visible and near-infrared range, i.e.,  $0.36\ \mu\text{m}$  and  $1.3\ \mu\text{m}$ , the critical height variation of the surface according to Rayleigh's formula for  $10^\circ$  incidence angle ( $\theta_i$ ) is between  $0.05\ \mu\text{m}$  and  $0.17\ \mu\text{m}$ , and for  $\theta_i=70^\circ$  is between  $0.13\ \mu\text{m}$  and  $0.47\ \mu\text{m}$ , respectively (Cierniewski and Courault 1993). Irregularities of a soil's surface at larger scales, caused by soil aggregates and clods, make it impossible to illuminate the whole surface directly. These elements produce shadow which becomes another important factor influencing the shape of the re-radiation pattern (Cierniewski 1987, 1989, Cooper and Smith 1985, Graetz and Gentle 1982, Huete 1987, Milton and Webb 1987, Norman *et al.* 1985, Pech *et al.* 1986, Ranson *et al.* 1985). Energy reflected from shaded soil fragments is many orders-of-magnitude smaller than energy leaving sunlit soil fragments. The degree of soil surface shadowing depends on the density of the elements which cast the shadow, the general configuration of the soil surface and its slope in relation to incident rays.

Several geometrical models have been proposed which predict soil reflectance based on the assumption that shadowing of soil aggregates or clods has a greater influence than the scattering properties of a soil material at the micro-scale. Soil aggregates in the model of Norman *et al.* (1985) were simulated by cuboids. Height of soil surfaces in the Monte Carlo reflectance model of Cooper and Smith (1985) varied periodically with the cosine function in one or two directions for 'row' and 'clump' soils, respectively. The models of Cierniewski (1987, 1989) and Irons *et al.* (1992) describe soil aggregates by regularly spaced equal-sized opaque spheres, while Cierniewski and Verbrughe's model (1994) simulates them by spheroids of a defined proportion of their vertical to horizontal radii. All the models assume only perfectly diffuse reflection from directly illuminated soil fragments.

A new model, taking into account the diffuse as well as the specular component of energy leaving soil surfaces in the visible and near-infrared, is used in this paper to describe the influence of soil surface roughness, caused by soil aggregates or soil clods, on the soil bidirectional reflectance distribution. The influence of soil surface roughness was analysed on artificially formed soil surfaces made of two spectrally different soil materials: a mineral loam of relatively high reflectance and a loam with high organic matter content and much lower reflectance. A deeper understanding of the interaction of electromagnetic radiation in the Vis-NIR domain with interpreted natural bare soils is important for a further improvement of remote sensing methods. The knowledge of the interaction mechanisms will enable us to find a way to correct satellite data for non constant illumination and viewing direction. It is particularly important for data of multiangles sensors of satellites as the SPOT (HRV), NOAA (AVHRR), or ERS (ATSR).

## 2. Methods

### 2.1. Soil reflectance model

The model predicts the reflectance distribution of a horizontal soil surface along the solar principal plane (SPP). Equal-sized opaque spheroids of horizontal ( $a$ ) and vertical ( $b$ ) radii lying on a horizontal surface simulate the soil surface. They are arranged on the surface so their centres in the horizontal projection are at a separation 'd'. The lower the relative distance ( $d$ ) to the radius ( $a$ ), the higher roughness of

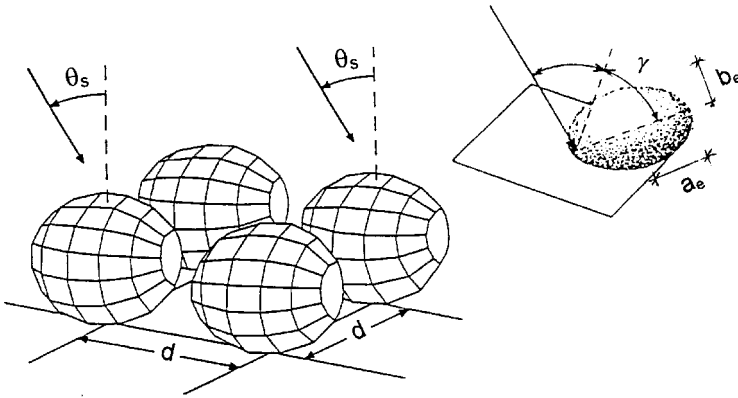


Figure 1. Geometry of the simulated soil surface and distribution of vectors of the near-perfect specular component of energy leaving one facet of the surface, where  $a_e$  and  $b_e$  are the major and the minor radius of the first component,  $\gamma$  is the angle of the reflected sunbeams to the normal and  $\theta_s$  is the solar zenith angle.

the simulated soil. The geometrical structure is illuminated by the direct solar beam at a zenith angle  $\theta_s$ , and diffuse skylight (figure 1).

In the first step the model calculates the area of illuminated ( $A_i$ ) and shaded ( $A_s$ ) facets of the given and the near spheroids and the ground between the spheroids, visible at a given view zenith ( $\theta_v$ ) angle of the sensor. The areas are determined analytically using trigonometrical equations.

In the second step the model calculates the electromagnetic energy coming to the individual facet of the geometrical structure. The slope angle of each facet ( $\beta$ ) and its azimuth angle ( $\phi_r$ ), together with the Sun zenith ( $\theta_s$ ) and azimuth ( $\phi_s$ ) angles, determine the amount of energy reaching the sunlit surface using the factor ( $E_{fa}$ ), defined as:

$$E_{fa} = \cos \theta_s \cos \beta + \sin \beta \sin \theta_s (\sin \phi_s \sin \phi_r + \cos \phi_s \cos \phi_r), \tag{1}$$

where  $\phi_s$  equals  $90^\circ$  for all the solar azimuth angles.

The factor  $E_{fa}$  expresses the cosine of the incidence angle ( $\gamma$ ) of the direct solar beam to the facet.

The model assumes that the energy leaving a given sunlit facet of the geometrical structures has a specular-diffuse character. A part of the direct energy is reflected as from a near-perfect specular object and a part as from a perfect diffuse one.

Light reflected from a given facet in the near-perfect specular way is dispersed into many directions creating a spheroidal shape of its distribution. The position of the major axis of the spheroid is into the direction of the reflected beam. The elongation of the spheroid ( $l_e$ ), defined as the proportion of its major radius ( $a_e$ ) to its minor radius ( $b_e$ ), depends on polarization ( $Fp_{(\gamma)}$ ) of the reflected light  $E_{fa}$  at the  $\gamma$  angle, as:

$$l_e = a_e/b_e = 1/(1 - Fp_{(\gamma)}); Fp_{(\gamma)} = r_{\perp}^2 - r_{\parallel}^2, \tag{2}$$

where  $r_{\perp}$  and  $r_{\parallel}$  are respectively the perpendicular and parallel Fresnel reflection

coefficients, given by:

$$r_{\perp}(\gamma) = (n\mu_T - \mu_I) / (n\mu_T + \mu_I) \text{ and } r_{=}(\gamma) = (n\mu_I - \mu_T) / (n\mu_I + \mu_T) \\ \text{with } \mu_I = \cos\gamma = E_{fa} \text{ and } \mu_T = (1 - \sin^2 \gamma / n^2)^{0.5}, \quad (3)$$

where  $n$  is the refractive index of the reflective medium.

The expression  $1/(1 - Fp_{(\gamma)})$  changes from 1 to infinite, describing respectively distributions of reflected light from perfectly diffuse to perfectly specular.

The volume of the spheroid ( $V_{sp}$ ):

$$V_{sp} = 4/3 \pi a_e b_e^2, \quad (4)$$

as a measure of reflected energy in the near-perfect specular way, is constant independent of its elongation. Knowing values of the spheroidal volume and the ratio between its major and minor axis we can calculate the magnitude of the light ( $e_{sp}$ ).

The component of energy leaving a given facet in the perfectly diffuse way is dispersed into equal-size magnitude ( $e_{di}$ ) creating the ideal shape of sphere of volume ( $V_{di}$ ):

$$V_{di} = 4/3 \pi (e_o/2)^3, \quad (5)$$

where  $e_o$  is a magnitude in direction perpendicular to the facet.

The magnitude of the  $e_{di}$  is calculated using the same assumption as for  $e_{sp}$ , but for a sphere. The proportion between the near-perfect specular and the perfect diffuse energy expresses the specular-diffuse coefficient (SDC):

$$SDC = V_{sp} / V_{di}. \quad (6)$$

The energy outgoing from a given sunlit facet ( $E_{ija}$ ), sensed by the sensor from the given direction ( $\theta_v$ ), is described by the coefficient:

$$E_{ija} = E_{fa} [SDC^{1/3} e_{sp} + (1 - SDC^{1/3}) e_{di}] + f_{di}, \quad (7)$$

where  $f_{di}$  is the ratio of skylight to direct light for the given wavelength, is proportional to the area of a given sunlit facet ( $A_{ija}$ ). The energy leaving the shaded facet ( $E_{Sfa}$ ), expressed by the  $f_{di}$  fraction of an isotropic distribution, is proportional to the area of shaded facet ( $A_{Sfa}$ ). The radiance factor of the simulated soil surface ( $L_{(\theta^v)}$ ) visible to the radiometer from the given direction ( $\theta_v$ ) can be formulated as:

$$L_{(\theta^v)} = \frac{\sum_{i=1}^j E_{ija} A_{ija} + \sum_{i=1}^j E_{Sfa} A_{Sfa}}{\sum_{i=1}^j A_{ija} + A_{Sfa}} \quad (8)$$

where  $i$  is  $i$ th facet of the geometrical structure visible inside of the field-of-view of the radiometer at angle  $\theta_v$ .

The reflectance of the simulated surface is finally expressed by the normalized reflectance ( $NR_{(\theta^v)}$ ) which is defined as the ratio of the total radiance measured from the off-nadir direction to the radiance measured from nadir.

The data generated by the model are compared with experimental spectral data collected on artificial soil surfaces in outdoor conditions.

## 2.2. Field experiment

Artificial rough soil surfaces used in the experiment consisted of spheres, made of air dry (to equilibrium with atmosphere) soil material using forms prepared from

ping-pong balls. The balls were dispersed on the same soil materials, flat and horizontally situated. The spheres were arranged so their centres in the horizontal projection were at the relative distance ( $d$ ) to their radius ( $a$ ) first 2, and then 4, representing respectively soil surfaces of high and medium density of soil aggregates or clods.

Spectral data of the surfaces were measured by a three-channel field radiometer CIMEL simulating the SPOT (HRV) bands (XS1: 0.50–0.59  $\mu\text{m}$ , XS2: 0.61–0.68  $\mu\text{m}$  and XS3: 0.79–0.89  $\mu\text{m}$ ). Radiance data were collected along the solar principal plane in 13 directions at view zenith angles from 60° towards the Sun through the nadir to 60° away from the Sun at 10° increments. The radiometer observed the soil surface from a distance of 2 m. This instrument with a 12° field-of-view (FOV) integrated reflected energy from a circular area which varied from 0.14 m<sup>2</sup> at a 0° view zenith angle to an elliptical area of 0.29 m<sup>2</sup> at 60° view zenith angle.

The spectral measurements were acquired in Poznan, Poland on 24 and 25 April 1994, under clear skies the solar zenith angle varied from 39° to 69°.

### 3. Results and discussion

The materials which were used to form the artificial soil surfaces are described in table 1.

The model calculated the normalized reflectance ( $NR_{(\theta)}$ ) along the solar principal plane for a given distance between soil aggregates, assuming that all horizontal fragments of the simulated surfaces visible by the radiometer at a given view zenith angle behaved like the smooth soil materials. Spectral data of the smooth surfaces were used to find the shape of a geometrical structure and their specular-diffuse coefficient (SDC) which could simulate their reflectance at definite illumination conditions. They were found by substituting different values into the model and looking for the values which give the highest coefficient of determination and the lowest root mean square error between the model-generated and measured soil reflectance data. The best SDC for the loam and loam with humus was 0.015 and 0.035, respectively. The smooth loam material was simulated by hemispheres of radius ' $a$ ' lying in the net of squares of distance  $d=3.75a$ , and the loam with humus by a similar structure of hemispheres, but at a distance  $d=4.5a$ .

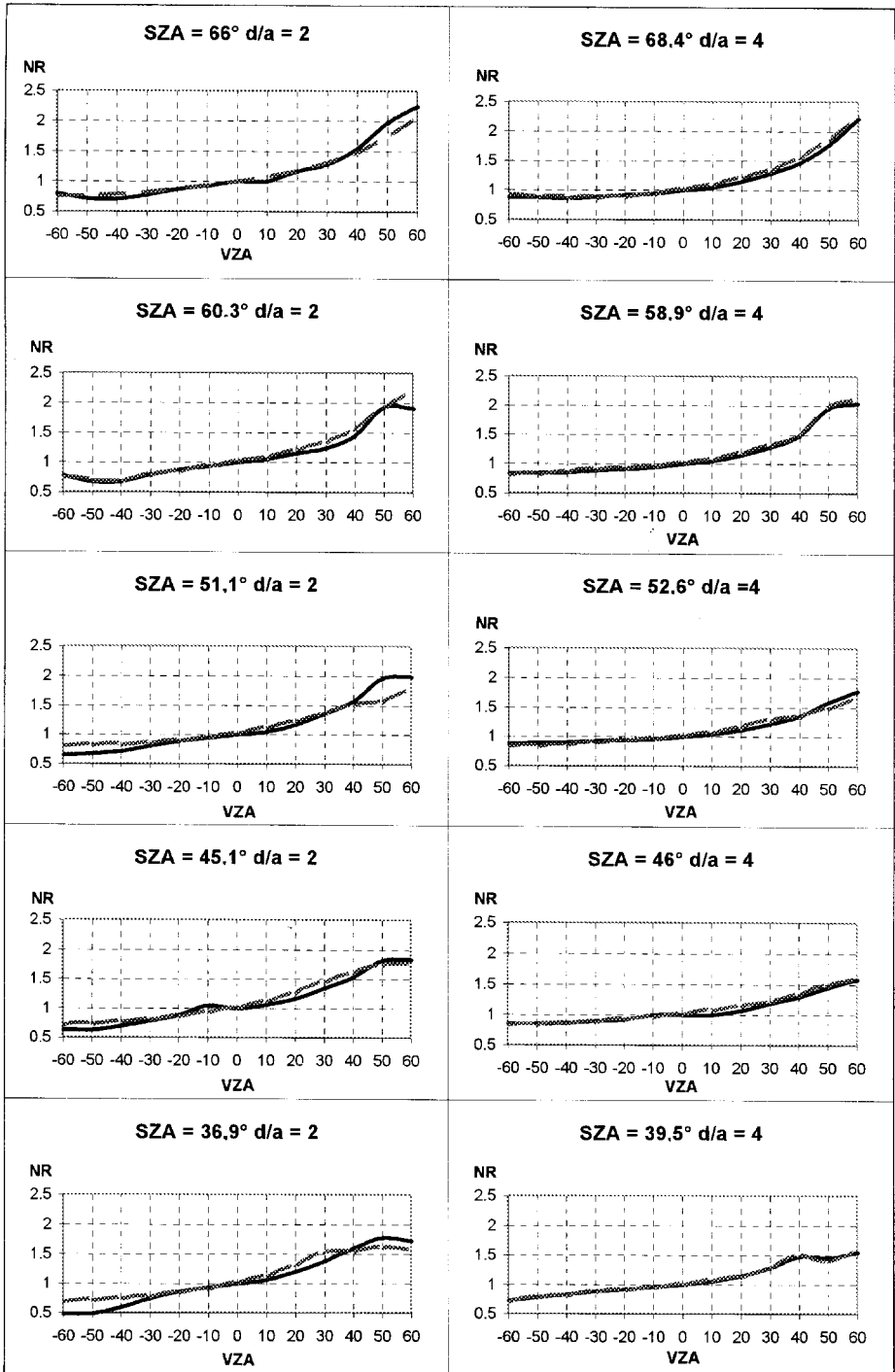
Strong correlation between measured and simulated reflectance data for the relative distance between the spheres  $d/a$  equals 2 and 4 enabled the application of the model to the simulation of the reflectance distribution for other distances (figures 2 and 3, table 2).

The distribution of the normalized reflectance (NR) along the solar principal plane (SPP) was simulated for aggregates of the sphere shape being at the relative  $d/a$  distance from 2 to 8 at 0.25 increments. The data were predicted for three zenithal

Table 1. Features of soil materials.

Material	Content in % of			Organic matter content (%)	Dry Munsell colour
	sand	silt	clay		
Mineral loamy	50	37	13	0	10YR6/4
Loamy with humus	56	32	12	4.7	10YR2/3

Loam



## Loam with humus

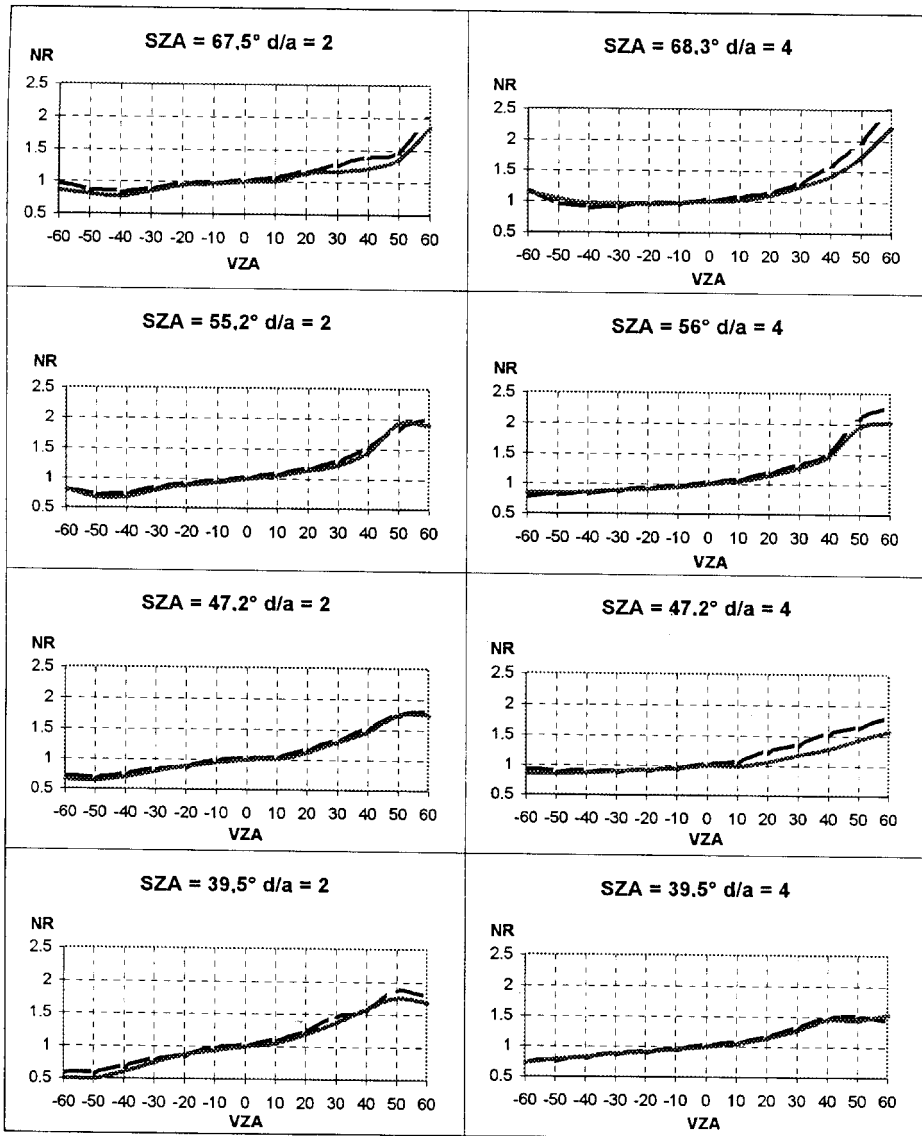


Figure 2. Relation between the normalized reflectance (NR) along the solar principal plane for the XS2 channel predicted by the model (solid line) and that measured (dashed line) for chosen soil surfaces for the given solar zenith angle (SZA).  $d/a$  is the relative distance between the soil aggregates to their horizontal radii ( $a$ ). Negative values of the view zenith angle (VZA) correspond to forward scattering directions and positive values to backscattering directions.

positions of the Sun:  $70^\circ$ ,  $50^\circ$  and  $30^\circ$ . They were generated using the refractive index ( $n$ ) of the soil material equal 1.51, 1.50 and 1.48 for XS1, XS2 and XS3, respectively, and for the fraction of skylight ( $f_{sk}$ ) equals 0.2 for XS1 and 0.15 for XS2 and XS3. The ' $n$ ' values were taken from the paper of Pollack, *et al.* (1973).

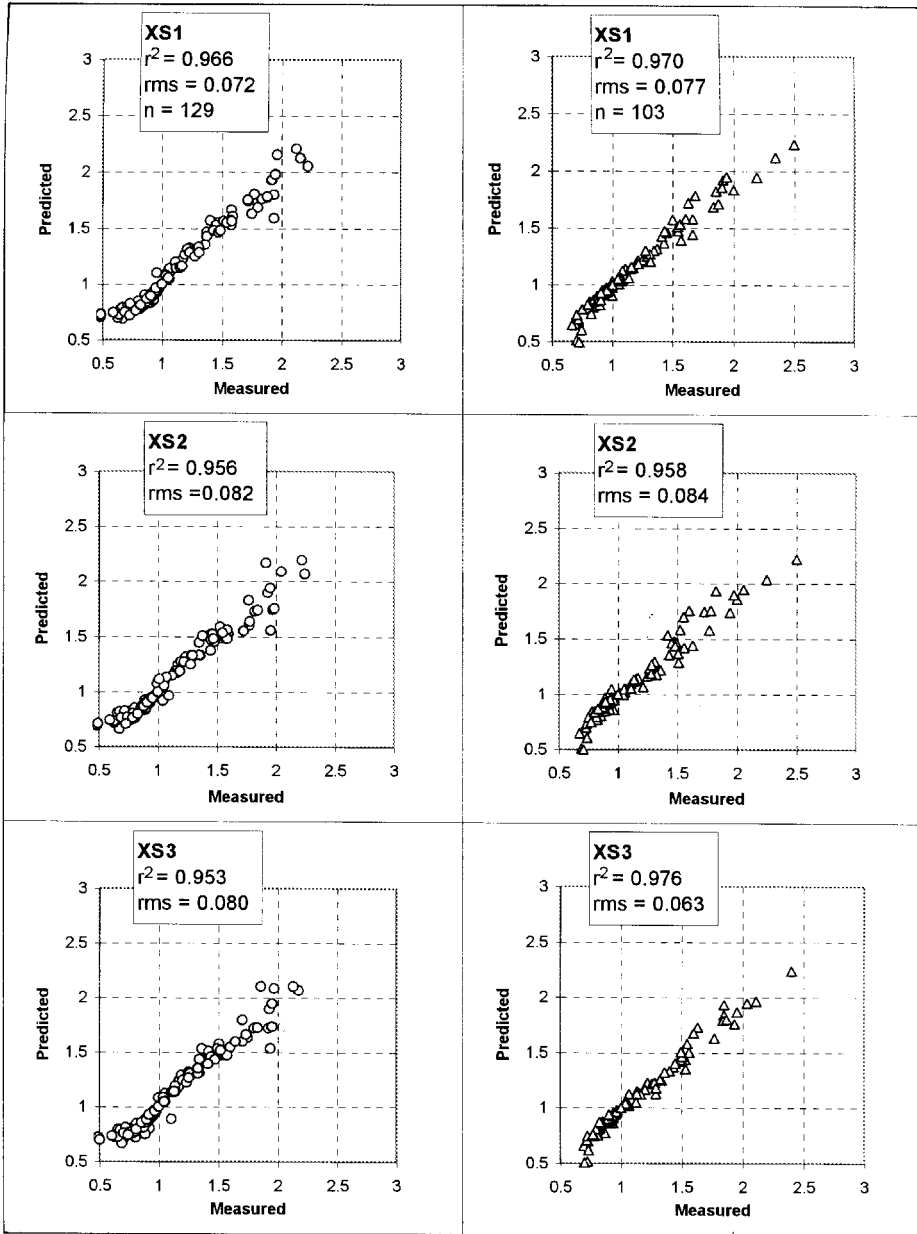


Figure 3. Relation between measured and predicted normalized reflectance for the loam (o) and loam with humus ( $\Delta$ ) materials for XS1, XS2 and XS3 channels of the radiometer.  $r^2$  is the coefficient of determination, rms is the root mean square error, while n is the number of analysed pairs of data.

Planes presenting the distribution of the NR along the SPP versus the relative distances between soil clods ( $d/a$ ) were similar for the three radiometer channels. Figure 4 shows the data for the XS2 channel.

Variation of the reflectance is clearly higher in the backscattering range than in

Table 2. Coefficient of determination ( $r^2$ ) and root mean square (rms) for measured and simulated soil surface reflectance data.

Material	Solar zenith angle ( $^\circ$ )	Relative distance $d/a$	SX1		Channels: SX2		SX3	
			$r^2$	rms	$r^2$	rms	$r^2$	rms
Mineral loamy	66	2	0.981	0.070	0.986	0.099	0.968	0.081
	66.8	4	0.971	0.076	0.994	0.116	0.980	0.067
	60.3	2	0.992	0.065	0.983	0.085	0.982	0.080
	58.9	4	0.998	0.040	0.998	0.023	0.995	0.040
	51.1	2	0.965	0.039	0.965	0.016	0.964	0.015
	52.6	4	0.989	0.038	0.969	0.064	0.985	0.043
	45.1	2	0.972	0.071	0.964	0.083	0.953	0.081
	46	4	0.997	0.029	0.959	0.052	0.941	0.072
	39.6	2	0.960	0.137	0.951	0.135	0.945	0.129
	39.5	4	0.998	0.014	0.980	0.041	0.997	0.016
	Loamy with humus	67.5	2	0.977	0.066	0.983	0.78	0.988
68.3		4	0.990	0.014	0.992	0.121	0.993	0.052
55.2		2	0.997	0.029	0.997	0.046	0.988	0.034
56		4	0.978	0.105	0.985	0.077	0.985	0.058
47.2		2	0.998	0.125	0.997	0.027	0.996	0.042
47.2		4	0.989	0.055	0.976	0.123	0.994	0.053
39.5		2	0.996	0.057	0.989	0.057	0.989	0.070
39.5		4	0.994	0.010	0.979	0.043	0.996	0.025

the forward scattering one. Generally, the higher the roughness of the soil surface, expressed by a lower distance between soil aggregates or clods, the higher the variation. The model predicts that at specific illumination conditions, especially for high solar zenith angles, soil surfaces with the minimum distance between soil aggregates can show lower variation of reflectance in the SPP than surfaces with a little lower roughness. Most shadow areas are on near-vertical sides of the soil aggregates. The areas are invisible for view directions near the nadir and also for more oblique directions, being covered by next adjoining aggregates. As a consequence, the soil surface seems to be brighter than for surfaces with higher aggregate distances. When soil aggregates are at slightly higher distances than the minimum, shadows cast on the horizontal ground between the aggregates visible by the sensor can significantly modify the distribution of the NR factor as a function of the view zenith angle. The reflectance data simulated for solar zenith angle (SZA)  $70^\circ$  clearly demonstrates this effect. For this illumination condition the highest variation is observed for the relative distance between aggregates  $d/a$  about 2.75. Symptoms of the effect are weakly visible SZA =  $50^\circ$  whilst for  $30^\circ$  they disappear completely. This effect predicted by the model may explain the results of Irons and Smith's (1990) studies, who observed that the roughest soil surface scattered radiation as strongly as the smoothest surface.

The results of the simulation show that for higher distances between soil aggregates or clods than  $d/a=3$ , the normalized reflectance (NR) decreases, becoming progressively similar to the distribution of reflectance for smooth surfaces without aggregates. Just before  $d/a=6$  this distribution starts to change very little and it approaches the distribution from smooth surfaces, even for a solar zenith angle of  $70^\circ$ .

Specular features of the analysed soil materials, show increased reflectance in the forward scattering range as the view zenith angle increases for high solar zenith

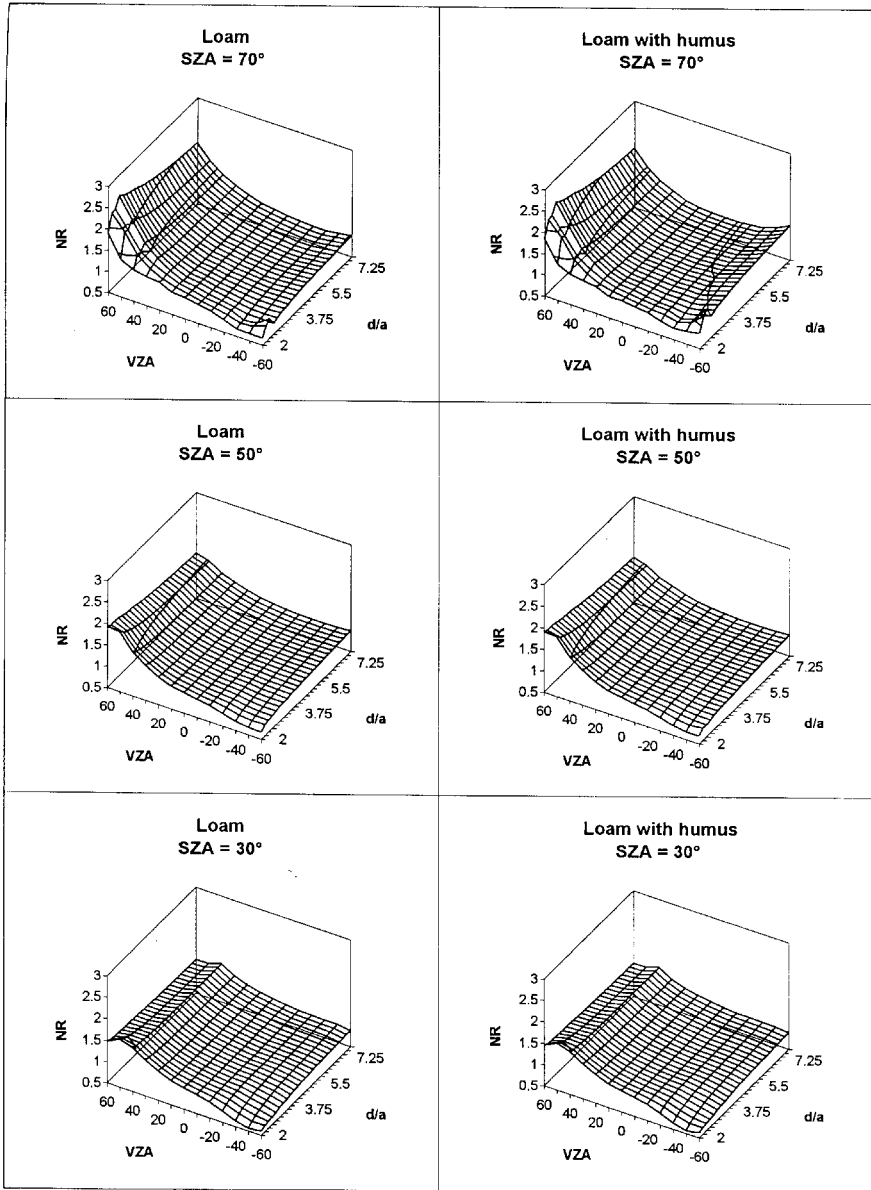


Figure 4. Relation predicted by the model between the normalized reflectance (NR) along the solar principal plane for the XS2 channel and the relative distance ( $d/a$ ) between soil aggregates for chosen solar zenith angle (SZA). Negative values of the view zenith angle (VZA) correspond to forward scattering directions and positive values to backscattering directions.

angles, especially for low roughness surfaces. When the relative distance between soil aggregates produces a small proportion of shadow, the shadowing area does not radically reduce the specular effects visible in the forward scattering range of the reflectance distribution. The behaviour of the measured and simulated soil surfaces accords with that noted by Mulders (1987), in that soil materials with a relatively

high content of organic matter have a higher proportion of specular component in the reflected energy than materials with a lower organic matter content.

#### 4. Conclusions

The results of the work, both the measurements and the simulation of the reflectance along the solar principal plane of rough soil surfaces formed with mineral loam and loam with humus materials, show higher reflectance in the backscattering range than in the forward scattering one. Generally, the higher the roughness of the surface, the greater the variation.

The model-generated data of reflectance suggest that for high solar zenith angles, soil surfaces of the highest roughness, expressed by the minimum distances between soil aggregates, can show lower variation of reflectance along the solar principal plane than soil surfaces of a little lower roughness.

The loamy soil material with high organic matter content demonstrated features of specular reflection at high solar zenith angles.

#### Acknowledgments

The authors thank Michal Farys, Slawomir Krolewicz and Wojciech Rosik for their help in preparation of the figures to the paper.

#### References

- CIERNIEWSKI, J., 1987, A model for soil surface roughness influence on the spectral response of bare soils in the visible and near-infrared range. *Remote Sensing of Environment*, **123**, 97–115.
- CIERNIEWSKI, J., 1989, The influence of the viewing geometry of bare rough soil surfaces on their spectral response in the visible and near-infrared range. *Remote Sensing of Environment*, **127**, 135–142.
- CIERNIEWSKI, J., and COURAULT, D., 1993, Bidirectional reflectance of bare soil surface in the visible and near-infrared range. *Remote Sensing Reviews*, **7**, 321–339.
- CIERNIEWSKI, J., and VERBRUGGHE, M., 1994, A geometrical model of soil bidirectional reflectance in the visible and near-infrared range. *Proceedings of 6th International Symposium on Physical Measurements and Signatures in Remote Sensing, 17–2 January 1994, Val d'Isère, France*: International Society for Photogrammetry and Remote Sensing, pp. 635–642.
- COOPER, K. D., and SMITH, J. A., 1985, A Monte Carlo reflectance model for soil surfaces with three-dimensional structure. *I.E.E.E. Transactions on Geoscience and Remote Sensing*, **23**, 668–673.
- DEERING, D. W., ECK, T. F., and OTTERMAN, J., 1990, Bidirectional reflectances of selected desert surfaces and their three-parameter soil characterization. *Agricultural and Forest Meteorology*, **1**, 71–93.
- GRAETZ, R. D., and GENTLE, M. R., 1982, A study of the relationship between reflectance characteristics in the Landsat wavebands and the composition and structure of an Australian semi-arid rangeland. *Photogrammetric Engineering and Remote Sensing*, **148**, 1721–1736.
- HUETE, A. R., 1987, Soil and Sun angle interactions on partial canopy spectra, *International Journal of Remote Sensing*, **18**, 1307–1317.
- IRONS, J. R., and SMITH, J. A., 1990, Soil surface roughness characterization from light scattering observations. *10th Annual International Geosciences and Remote Sensing Symposium II*, pp. 1007–1010.
- IRONS, J. R., CAMPBELL, G. S., NORMAN, J. M., GRAHAM, D. W., and KOVALICK, W. M., 1992, Prediction and measurement of soil bidirectional reflectance. *I.E.E.E. Transactions on Geoscience and Remote Sensing*, **30**, 249–260.

- KIMES, D. S., and SELLERS, P. J., 1985, Inferring hemispherical reflectance of the Earth's surface for global energy budget from remotely sensed nadir or directional radiance values. *Remote Sensing of Environment*, **118**, 205–223.
- MILTON, E. J., and WEBB, J. P., 1987, Ground radiometry and airborne multispectral survey of bare soils. *International Journal of Remote Sensing*, **18**, 3–14.
- MULDERS, M. A., 1987, *Remote Sensing in Soil Science* (Amsterdam, Oxford, New York, Tokyo: Elsevier).
- NORMAN, J. M., WELLES, J. M., and WALTER, E. A., 1985, Contrast among bidirectional reflectance of leaves, canopies, and soils. *I.E.E.E. Transactions on Geoscience and Remote Sensing*, **23**, 659–667.
- OTT, W., PFEIFFER, B., and QUIEL, F., 1984, Directional reflectance properties determined by analysis of airborne multispectral scanner data and atmospheric correction. *Remote Sensing of Environment*, **116**, 47–54.
- POLLACK, J. B., TOON, O. B., and KHARE, B. N., 1973, Optical properties of some terrestrial rocks and glasses. *Icarus*, **19**, 372–389.
- PECH, R. P., GRAETZ, R. R., and DAVIS, A. W., 1986, Reflectance modelling and the derivation of vegetation indices for an Australian semi-arid shrubland. *International Journal of Remote Sensing*, **17**, 389–403.
- RANSON, K. J., BIEHL, L. L., and BAUER, M. E., 1985, Variation in spectral response of soybeans with respect to illumination, view and canopy geometry. *International Journal of Remote Sensing*, **16**, 1827–1842.